Nonlinear nonreciprocal transport in antiferromagnets free from spin-orbit coupling

Satoru Hayami and Megumi Yatsushiro

Department of Applied Physics, The University of Tokyo, Tokyo 113-8656, Japan
and Department of Physics, Hokkaido University, Sapporo 060-0810, Japan

We theoretically propose a realization of nonlinear nonreciprocal transport in antiferromagnets without relying on the relativistic spin-orbit coupling. Through symmetry and microscopic model analyses, we show that a local spin scalar chirality inducing an asymmetric band modulation becomes a source of a Drude-type nonlinear transport, while an electric polarization induced by a collinear spin configuration in a triangle unit leads to a Berry-curvature-dipole-type nonlinear transport. We demonstrate $120°$ antiferromagnetic ordering on a triangular lattice and a breathing kagome lattice in an external magnetic field as typical examples. Our results open another direction for the design and engineering of functional materials to show rich parity-violating transport phenomena induced by spontaneous magnetic phase transitions even without the spin-orbit coupling.

I. INTRODUCTION

The study of magnetism has long been the subject of considerable theoretical and experimental interest in condensed matter physics. Once a spontaneous magnetic phase transition occurs, a variety of intriguing physical phenomena appear as a consequence of the interplay between charge and spin degrees of freedom in electrons, such as the magnetoelectric effect irrespective of metals and insulators [1–11]. In addition, the topological aspect of magnetic orderings has been extensively studied in recent years since the discovery of magnetic skyrmions [12–15] and magnetic topological insulators [16–19]. These diverse physical properties in magnetic systems provide us a promising possibility for potential applications to functional spintronics devices [20–22].

Toward applications, it is significant to elucidate the conditions to induce physical phenomena at the fundamental level. The symmetry aspect provides their macroscopic conditions. Meanwhile, fundamental understanding of the microscopic origins is important to realize an efficient bottom-up design of functional magnetic materials. One of the successes has been achieved in the anomalous Hall effect in magnetic materials [23,24]. Although it was originally discussed in ferromagnets with the relativistic spin-orbit coupling (SOC) [25–30], unconventional mechanisms in collinear [31–36], noncollinear [37–42], and noncoplanar [43–47] antiferromagnets (AFMs) have been clarified based on the Berry curvature [48–52] and multipoles [36,40]. Among them, noncoplanar spin textures give rise to the anomalous (topological) Hall effect even without either SOC or uniform magnetic moments, which results in broadening the scope of materials [44,46,53,54].

The rich physics brought about by the anomalous Hall effect leads to a natural extension to a nonlinear nonreciprocal transport beyond the linear response. Although the framework and the symmetry argument for the nonreciprocal transport have been developed [55–63], few studies have focused on the microscopic mechanisms in magnetic systems [64–72].

Especially, the effect of SOC can be incorporated in most cases, which narrows down candidate materials.

In this paper, we explore another mechanism of the nonlinear nonreciprocal transport in AFMs without relying on the SOC. Based on the symmetry and model analyses, we derive a microscopic essence for nonlinear nonreciprocal transports of Drude type and of Berry curvature dipole (BCD) type, which appear under different conditions: Drude-type nonlinear transport is induced by a noncoplanar spin configuration with the local spin scalar chirality, while BCD-type nonlinear transport is induced by a collinear spin configuration in a triangle unit with electric polarization. The results are demonstrated by examining three-sublattice $120°$ AFM orderings on a triangular lattice (TL) and a breathing kagome lattice (BKL) in an external magnetic field. We also discuss necessary conditions for model parameters to cause these nonlinear conductivities from the microscopic viewpoint. Our results indicate that noncollinear and noncoplanar magnetic orderings in frustrated and itinerant magnets with negligibly small SOC are also potential candidates to bring about rich parity-violating transport phenomena, which will stimulate further exploration of functional magnetic materials.

The rest of this paper is organized as follows. In Sec. II, we present a tight-binding model without the SOC on the TL and BKL, which consists of the hopping, the site-dependent AFM mean field, and an external magnetic field. We show the numerical results of the nonreciprocal transport for both lattice systems in Sec. III. We also discuss the important model parameters to induce the Drude-type and BCD-type nonlinear transports. Section IV is devoted to a summary.

II. MODEL

Let us start with a tight-binding model on the TL, which is given by

$$\mathcal{H}^{\mathrm{TL}} = -t \sum_{\langle ij \rangle \sigma} c_{i\sigma}^{\dagger} c_{j\sigma} + \sum_{i\sigma\sigma'} (\boldsymbol{h}_i + \boldsymbol{H}) \cdot c_{i\sigma}^{\dagger} \boldsymbol{\sigma}_{\sigma\sigma'} c_{i\sigma'}, \quad (1)$$
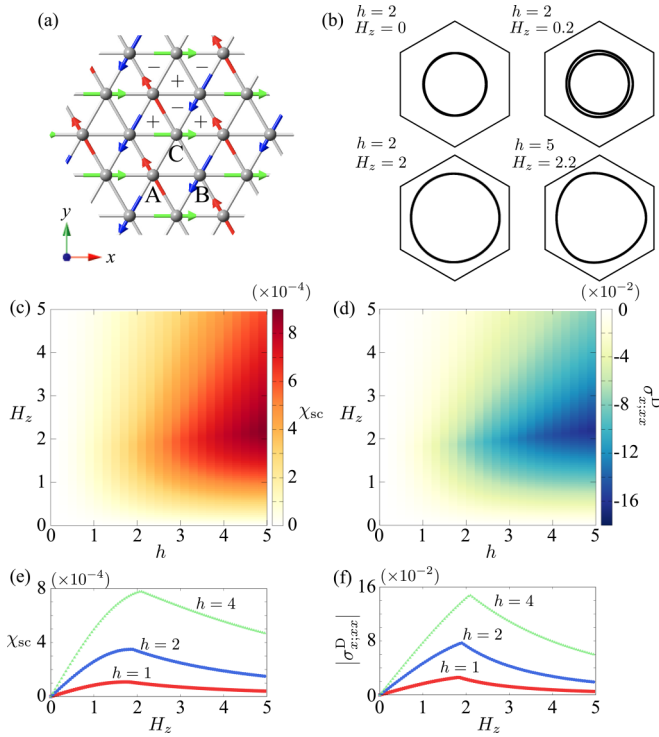
FIG. 1. (a) 120°-AFM structure on the TL. Here, $+$ or $-$ on the triangle represents the sign of the local spin scalar chirality $\chi_{\rm sc}$ under H_z. (b) Fermi surfaces at 1/10 filling for several h and H_z. (c) and (d) Contour plots of $\chi_{\rm sc}$ (c) and $\sigma^{\rm D}_{x;xx}$ (d) in the plane of h and H_z at 1/10 filling. (e) and (f) H_z dependences of $\chi_{\rm sc}$ (e) and $\sigma^{\rm D}_{x;xx}$ (f) for several h.

where $c^{\dagger}_{i\sigma}$ ($c_{i\sigma}$) is the creation (annihilation) operator for site i and spin $\sigma = \uparrow, \downarrow$. The first term represents the hoppings between the nearest-neighbor sites. The second term consists of the site-dependent AFM mean-field term $\boldsymbol{h}_i$ that originates from the Coulomb interaction U and an external magnetic field $\boldsymbol{H} = (0, H_y, H_z)$ in the yz plane, where $\boldsymbol{\sigma}$ is the vector of the Pauli matrices; the magnitude of $\boldsymbol{h}_i$ is roughly given by Um_i within the mean-field approximation in the single-band Hubbard model, where m_i represents the expectation value of the spins ($0 < m_i \leqslant 0.5$). For the former, we assume the noncollinear three-sublattice 120°-AFM structure consisting of $\boldsymbol{h}_{\rm A} = h(-1/2, \sqrt{3}/2, 0)$, $\boldsymbol{h}_{\rm B} = h(-1/2, -\sqrt{3}/2, 0)$, and $\boldsymbol{h}_{\rm C} = h(1, 0, 0)$ shown in Fig. 1(a), with amplitude h, to focus on the emergence of the nonreciprocal transport under noncollinear magnetic orderings. Such a noncollinear ordering is stabilized in the competing exchange interactions with the triangle unit in the itinerant electron models including not only the Hubbard model but also the periodic Anderson model and the classical Kondo lattice model [73–77] or in the magnetic anisotropy. We set $t = 1$ as the energy unit, take the lattice constant as unity, and consider the low 1/10 filling so that the Fermi surfaces consisting of two almost energetically degenerate bands become a simple shape, as shown in Fig. 1(b). In addition, to cover the situation from a weak-correlation regime ($U/t \ll 1$) to a strong-correlation regime ($U/t \sim 10$), h is changed from 0 to 5, as discussed in Sec. III A.
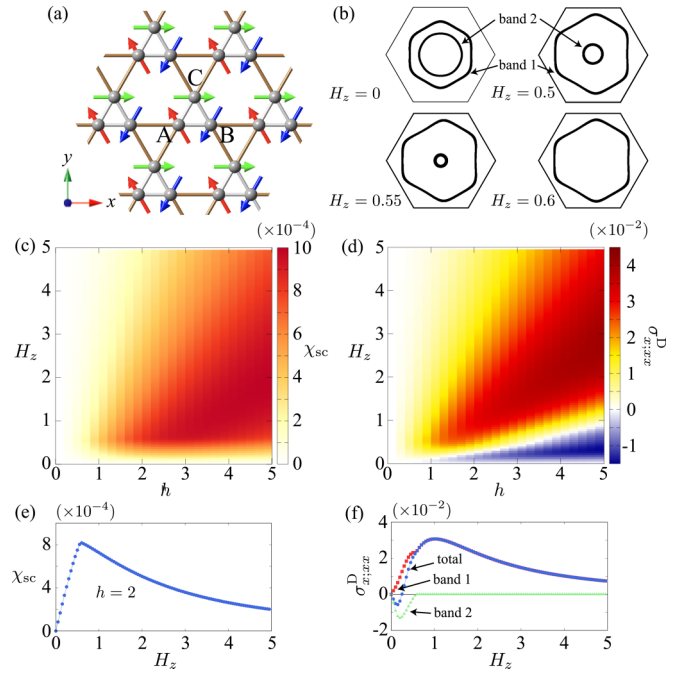

FIG. 2. (a) 120°-AFM structure in the BKL system. (b) Fermi surfaces at 1/10 filling for several H_z at $h = 3$. (c) and (d) Contour plots of $\chi_{\rm sc}$ (c) and $\sigma^{\rm D}_{x;xx}$ (d) in the plane of h and H_z at 1/10 filling. (e) and (f) H_z dependences of $\chi_{\rm sc}$ (e) and $\sigma^{\rm D}_{x;xx}$ (f) for $h = 2$. In (b) and (f), band 1 and band 2 represent the contributions from the lowest and second-lowest bands, respectively.

In the BKL system, the Hamiltonian is given by

$$\mathcal{H}^{\rm BKL} = -\left(t_a \sum_{\langle ij\rangle\sigma}^{\in\triangle} + t_b \sum_{\langle ij\rangle\sigma}^{\in\triangledown} \right) c^{\dagger}_{i\sigma} c_{j\sigma}$$
$$+ \sum_{i\sigma\sigma'} (\boldsymbol{h}_i + \boldsymbol{H}) \cdot c^{\dagger}_{i\sigma} \boldsymbol{\sigma}_{\sigma\sigma'} c_{i\sigma'}, \qquad (2)$$

where t_a (t_b) represents the hopping within upward (downward) triangles. Similar to the TL system, we consider the noncollinear three-sublattice 120°-AFM structure consisting of $\boldsymbol{h}_{\rm A} = h(-1/2, \sqrt{3}/2, 0)$, $\boldsymbol{h}_{\rm B} = h(-1/2, -\sqrt{3}/2, 0)$, and $\boldsymbol{h}_{\rm C} = h(1, 0, 0)$ shown in Fig. 2(a). We take the length of both triangles as unity, whose difference is expressed as the different hoppings; $t_a = 1$ and $t_b = 0.5$. The results are shown in Sec. III B.

III. RESULTS

We show the results of the TL system in Sec. III A and those of the BKL system in Sec. III B. We also discuss the essential model parameters for the Drude-type and BCD-type nonlinear transports in Sec. III C.

A. Triangular-lattice system

The 120°-AFM structure on the TL breaks the spatial inversion symmetry. Then, the antisymmetric spin polarization appears in the band structure in the model in Eq. (1) [78–80]. When the magnetic moments are on the xy plane under $\boldsymbol{H} = \boldsymbol{0}$, the antisymmetric z-spin polarization satisfying

threefold rotational symmetry occurs in the form of $k_x(k_x^2 - 3k_y^2)\sigma_z$ ($\boldsymbol{k}$ is the wave vector). In such a situation, the product symmetry of the sixfold rotation and the space-time-inversion operation remains, which results in the sixfold-symmetric Fermi surface. When introducing the magnetic field along σ_z, the asymmetry in terms of $+\boldsymbol{k}$ and $-\boldsymbol{k}$ appears [78,79]; the sixfold rotational symmetry of the Fermi surface is lost, as shown for several values of h and H_z in Fig. 1(b), where one of the two bands is away from the Fermi level while increasing H_z. Such an asymmetric band structure becomes the microscopic key ingredient to cause the Drude-type nonreciprocal nonlinear transport discussed below.

The Drude-type nonlinear conductivity $\sigma_{\eta;\mu\nu}^{\mathrm{D}}$ in $J_\eta = \sigma_{\eta;\mu\nu}^{\mathrm{D}} E_\mu E_\nu$ for $\eta, \mu, \nu = x, y, z$ is derived from the second-order Kubo formula as

$$\sigma_{\eta;\mu\nu}^{\mathrm{D}} = -\frac{e^3\tau^2}{2\hbar^3 N_{\boldsymbol{k}}} \sum_{\boldsymbol{k},n} f_{n\boldsymbol{k}} \partial_\eta \partial_\mu \partial_\nu \varepsilon_{n\boldsymbol{k}}, \qquad (3)$$

where e, τ, $\hbar$, and $N_{\boldsymbol{k}}$ are the electron charge, the relaxation time, the reduced Planck constant, and the number of supercells, respectively; we take $e = \tau = \hbar = 1$. $\varepsilon_{n\boldsymbol{k}}$ and $f_{n\boldsymbol{k}}$ are the eigenenergy and the Fermi distribution function with the band index n, respectively. $\sigma_{\eta;\mu\nu}^{\mathrm{D}}$ arises for nonzero $\partial_\eta \partial_\mu \partial_\nu \varepsilon_{n\boldsymbol{k}}$, i.e., for an asymmetrically deformed energy band. In the present 120° AFM in the two-dimensional TL system, $\sigma_{x;xx}^{\mathrm{D}} = -\sigma_{x;yy}^{\mathrm{D}} = -\sigma_{y;xy}^{\mathrm{D}}$ from the symmetry under H_z. Hereinafter, we fix the temperature $T = 0.01$ and $N_{\boldsymbol{k}} = 4800^2$.

Figures 1(c) and 1(d) show the color plots of χ_{sc} and $\sigma_{x;xx}^{\mathrm{D}}$ while changing h and H_z at $H_y = 0$, respectively. The local scalar chirality χ_{sc} is defined by $\chi_{\mathrm{sc}} = \langle \boldsymbol{s}_i \rangle \cdot (\langle \boldsymbol{s}_j \rangle \times \langle \boldsymbol{s}_k \rangle)$ where $\langle \boldsymbol{s}_i \rangle = (1/2)\langle \sum_{\sigma\sigma'} c_{i\sigma}^\dagger \boldsymbol{\sigma}_{\sigma\sigma'} c_{i\sigma'} \rangle$, $\langle \cdots \rangle$ is the expectation value, and i, j, and k are the sites in the triangle in the counterclockwise order. Comparing χ_{sc} in Fig. 1(c) with $|\sigma_{x;xx}^{\mathrm{D}}|$ in Fig. 1(d), one finds that there is a correlation between them in the wide range of h and H_z; both quantities increase while increasing h at fixed H_z, while they become the largest at intermediate H_z at fixed h [Figs. 1(e) and 1(f)]. This indicates that large $|\sigma_{x;xx}^{\mathrm{D}}|$ in AFMs without SOC can be realized when the noncoplanarity of the spin configuration becomes large.

Let us discuss the relationship between the nonreciprocal transport, the local scalar chirality, and the asymmetric band structure for an intuitive understanding. The microscopic origin of the nonzero $\sigma_{x;xx}^{\mathrm{D}}$ is understood from the distribution of the local spin scalar χ_{sc}. As shown in Fig. 1(a), the 120° AFM under H_z leads to the staggered alignment of $\pm\chi_{\mathrm{sc}}$ so that the sixfold rotational symmetry of the system is broken in the real-space picture. Accordingly, the sixfold symmetry of the Fermi surfaces is also broken, which leads to the asymmetric band deformation. The important point is that the uniform component of χ_{sc} is not necessary to induce nonreciprocal transport; the essence lies in its spatial distribution breaking the sixfold rotational symmetry. Thus the relationship between χ_{sc} and $\sigma_{x;xx}^{\mathrm{D}}$ is qualitatively different from that between χ_{sc} and the linear topological Hall effect, the latter of which requires the uniform alignment of χ_{sc}.

B. Breathing-kagome-lattice system

A similar correlation between χ_{sc} and $\sigma_{x;xx}^{\mathrm{D}}$ also occurs in other noncollinear AFMs. To demonstrate that, we investigate the 120° AFM ordering in the BKL structure in Fig. 2(a), where the model Hamiltonian is given by Eq. (2). The 120° AFM ordering in Fig. 2(a) exhibits the asymmetric band deformation in the form of $k_x(k_x^2 - 3k_y^2)$ when χ_{sc} is present under H_z, as shown by the Fermi surfaces at 1/10 filling and $h = 3$ in Fig. 2(b); two bands denoted as bands 1 and 2 form the Fermi surfaces for small H_z, and band 2 is away from the Fermi level while increasing H_z.

The asymmetric band deformation under nonzero χ_{sc} leads to nonzero $\sigma_{x;xx}^{\mathrm{D}}$. Similar to the TL case in Sec. III A, the behaviors of $\sigma_{x;xx}^{\mathrm{D}}$ against h and H_z in Fig. 2(d) have a correspondence to χ_{sc} in Fig. 2(c) except for the small-H_z region [see also the case at $h = 2$ in Figs. 2(e) and 2(f)]. The deviation for small H_z is owing to the opposite-sign contributions from the two Fermi surfaces, where the negative contribution from band 2 is larger than the positive one from band 1, as shown in Fig. 2(f).

On the other hand, the 120° AFM ordering in the BKL structure exhibits another nonreciprocal transport, which is referred to as the nonlinear Hall effect. The nonlinear Hall conductivity is calculated by

$$\sigma_{\eta;\mu\nu}^{\mathrm{BCD}} = \frac{e^3\tau}{2\hbar^2 N_{\boldsymbol{k}}} \sum_{\boldsymbol{k},n} f_{n\boldsymbol{k}} \epsilon_{\eta\mu\lambda} D_n^{\nu\lambda}(\boldsymbol{k}) + [\mu \leftrightarrow \nu], \qquad (4)$$

where $D_n^{\mu\nu}(\boldsymbol{k})$ represents the BCD derived from the Berry curvature $\Omega_n^\nu(\boldsymbol{k})$; $D_n^{\mu\nu}(\boldsymbol{k}) = \partial_\mu \Omega_n^\nu(\boldsymbol{k})$ [56]. In contrast to $\sigma_{\eta;\mu\nu}^{\mathrm{D}}$, $\sigma_{\eta;\mu\nu}^{\mathrm{BCD}}$ does not require the breaking of the time-reversal symmetry; the breakings of the spatial inversion symmetry and threefold rotational or mirror symmetry to activate the rank-1 electric dipole and rank-2 electric toroidal quadrupole are important [56,62,63,81]. Although there is no finite component of $\sigma_{\eta;\mu\nu}^{\mathrm{BCD}}$ in the TL system under any magnetic fields since such multipole degrees of freedom are not activated, it becomes finite in the BKL system owing to the active electric dipoles under the in-plane field, as discussed below. For example, in the case of H_y, nonzero components of $\sigma_{\eta;\mu\nu}^{\mathrm{BCD}}$ are given by $2\sigma_{x;yy}^{\mathrm{BCD}} = -\sigma_{y;xy}^{\mathrm{BCD}}$ and $2\sigma_{y;xx}^{\mathrm{BCD}} = -\sigma_{x;xy}^{\mathrm{BCD}}$ from the symmetry viewpoint.

The numerical results of two components, $\sigma_{y;xx}^{\mathrm{BCD}}$ and $\sigma_{x;yy}^{\mathrm{BCD}}$, while changing h and H_y at $H_z = 0$, are shown by the color maps in Figs. 3(a) and 3(b), respectively. The overall feature in both cases seems to be similar; there is a sign change while changing H_y for fixed h, and their absolute values are enhanced in the vicinity of the region where their sign change occurs, as shown in the inset of Fig. 3(b) at $h = 5$.

The enhancement of $\sigma_{y;xx}^{\mathrm{BCD}}$ is attributed to the change in the Fermi-surface topology by the band crossing. Figure 3(c) shows the change in the Fermi surfaces while increasing H_y at $h = 5$. We also plot the $\boldsymbol{k}$-resolved $\sigma_{y;xx}^{\mathrm{BCD}}(\boldsymbol{k})$ defined by $\sigma_{y;xx}^{\mathrm{BCD}} = \sum_{\boldsymbol{k}} \sigma_{y;xx}^{\mathrm{BCD}}(\boldsymbol{k})$ to represent the dominant contribution to $\sigma_{y;xx}^{\mathrm{BCD}}$ in momentum space. There are two Fermi surfaces in the low field, as shown in the case of $H_y = 0.06$. While increasing H_y, the two Fermi surfaces tend to merge at two $\boldsymbol{k}$ points, where $\sigma_{y;xx}^{\mathrm{BCD}}(\boldsymbol{k})$ is critically enhanced as shown at $H_y = 0.14$. Further increase in H_y leads to the decrease in
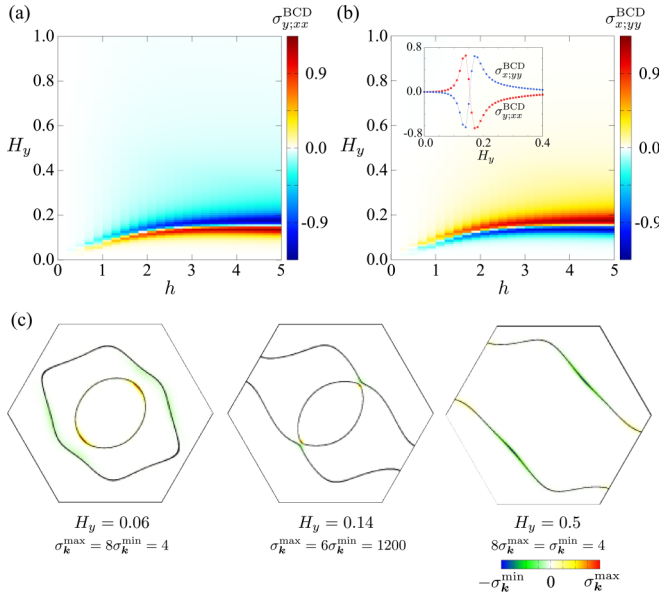
FIG. 3. (a) and (b) Contour plots of $\sigma_{y;xx}^{\mathrm{BCD}}$ (a) and $\sigma_{x;yy}^{\mathrm{BCD}}$ (b) in the plane of h and H_y at 1/10 filling. The inset of (b) represents the H_y dependence at $h = 5$ in (a) and (b). (c) Contour plots of $\sigma_{y;xx}^{\mathrm{BCD}}(\boldsymbol{k})$ projected onto the Fermi surfaces for several H_y at $h = 5$.

$\sigma_{y;xx}^{\mathrm{BCD}}$, as the lowest band is separated from the others. A similar discussion holds for $\sigma_{x;yy}^{\mathrm{BCD}}$.

The origin of $\sigma_{x;yy}^{\mathrm{BCD}}$ and $\sigma_{y;xx}^{\mathrm{BCD}}$ is due to the emergence of the electric polarization induced by spin-dependent kinetic motion of electrons under the spin arrangement in the triangle unit, where the electric polarization $\boldsymbol{P} = (P_x, P_y)$ in each upward triangle is given by $P_x \sim \langle s_{\mathrm{C}} \rangle \cdot (\langle s_{\mathrm{A}} \rangle - \langle s_{\mathrm{B}} \rangle)$ and $P_y \sim \langle s_{\mathrm{C}} \rangle \cdot (\langle s_{\mathrm{A}} \rangle + \langle s_{\mathrm{B}} \rangle) - 2 \langle s_{\mathrm{A}} \rangle \cdot \langle s_{\mathrm{B}} \rangle$. As the effective hopping amplitudes are different depending on the bonds connected by the parallel or antiparallel spin pairs, the induced spin moments become inequivalent, which results in $\boldsymbol{P}$. It is noted that a similar electric polarization in the triangle unit has also been discussed in Mott insulators [82]. When $H_z \neq 0$ but $H_y = 0$ under the 120° spin configuration, both P_x and P_y become zero, which results in $\sigma_{\eta;\mu\nu}^{\mathrm{BCD}} = 0$. Meanwhile, the in-plane magnetic field H_y deforms the 120° spin configuration to have nonzero P_x and P_y. As P_x and P_y have the same symmetry as $\sigma_{x;yy}^{\mathrm{BCD}}$ and $\sigma_{y;xx}^{\mathrm{BCD}}$, respectively, a nonzero nonlinear Hall effect appears. It is noted that the nonlinear Hall effect does not appear in the TL system, since both P_x and P_y are canceled out by considering the contributions from upward and downward triangles.

The above consideration indicates that the nonlinear Hall effect is induced even in the collinear spin configuration; it does not require the noncollinear spin configuration. Indeed, the x-spin (y-spin) component in $\boldsymbol{h}_i$ in addition to the uniform y-spin component from H_y is enough to induce P_y (P_x and P_y). In other words, $\sigma_{y;xx}^{\mathrm{BCD}}$ still remains nonzero when dropping either of the spin components, i.e., $h_{\mathrm{A}}^x = h_{\mathrm{B}}^x = h_{\mathrm{C}}^x = 0$ or $h_{\mathrm{A}}^y = h_{\mathrm{B}}^y = h_{\mathrm{C}}^y = 0$, while $\sigma_{x;yy}^{\mathrm{BCD}}$ becomes nonzero only when $h_{\mathrm{A}}^x = h_{\mathrm{B}}^x = h_{\mathrm{C}}^x = 0$ [83]. Thus the collinear spin configuration in the triangle unit is a minimal ingredient to induce the nonlinear Hall effect in the absence of SOC.
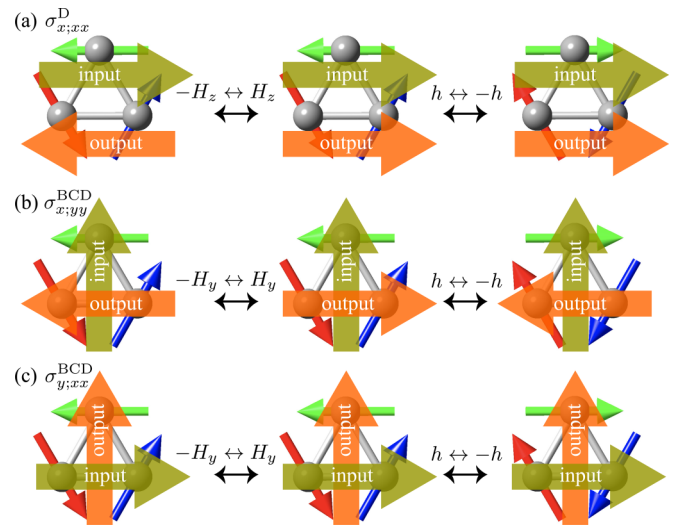

FIG. 4. Schematics to represent the behaviors of (a) $\sigma_{x;xx}^{\mathrm{D}}$, (b) $\sigma_{x;yy}^{\mathrm{BCD}}$, and (c) $\sigma_{y;xx}^{\mathrm{BCD}}$ when reversing the sign of the magnetic field (H_z or H_y) or the order parameter h.

C. Essential model parameters

Finally, let us discuss the essential model parameters to induce $\sigma_{\eta;\mu\nu}^{\mathrm{D}}$ and $\sigma_{\eta;\mu\nu}^{\mathrm{BCD}}$ from the microscopic viewpoint. Although the above results indicate that both h and H_z (or H_y) are important to induce the nonlinear conductivity, these dependences differ from each other. To show this, we calculate the essential model parameters based on the method in Ref. [63], which is given by $\sum_{ijk} C^{ijk} \sum_{\boldsymbol{k}} \mathrm{Tr}[v_{\eta\boldsymbol{k}} h^i(\boldsymbol{k}) v_{\mu\boldsymbol{k}} h^j(\boldsymbol{k}) v_{\nu\boldsymbol{k}} h^k(\boldsymbol{k})]$ for $\eta, \mu, \nu = x, y$, where C^{ijk} is the model-independent coefficient, $h^i(\boldsymbol{k})$ is the ith power of the Hamiltonian matrix at wave vector $\boldsymbol{k}$, and $v_{\eta\boldsymbol{k}}$ is the η component of the velocity operator; $\sigma_{\eta;\mu\nu}^{\mathrm{D}}$ ($\sigma_{\eta;\mu\nu}^{\mathrm{BCD}}$) is proportional to the real (imaginary) part of the trace.

For the Drude-type nonlinear conductivity, the essential factors of $\sigma_{x;xx}^{\mathrm{D}}$ in the TL and BKL systems are extracted as $h^2 H_z t^3$ and $h^2 H_z (t_a - t_b)$, respectively. This indicates that the AFM domain formation is irrelevant to $\sigma_{x;xx}^{\mathrm{D}}$, while the opposite field, $H_z \to -H_z$, reverses the sign of $\sigma_{x;xx}^{\mathrm{D}}$, as shown in Fig. 4(a). This means that the sign of χ_{sc} determines the direction of the output current. In addition, nonzero $\sigma_{x;xx}^{\mathrm{D}}$ is induced by $t_a \neq t_b$ in the BKL system, since spatial inversion symmetry is preserved when $t_a = t_b$. The BCD-type nonlinear conductivities, $\sigma_{x;yy}^{\mathrm{BCD}}$ and $\sigma_{y;xx}^{\mathrm{BCD}}$ in the BKL system, show different dependences regarding h and H_y; $\sigma_{x;yy}^{\mathrm{BCD}}$ is proportional to $h H_y (t_a - t_b)$, while $\sigma_{y;xx}^{\mathrm{BCD}}$ is $h^2 H_y^2 (t_a - t_b)$. In other words, $\sigma_{x;yy}^{\mathrm{BCD}}$ is reversed by reversing H_y or h, while $\sigma_{y;xx}^{\mathrm{BCD}}$ is invariant for such a change, as shown in Figs. 4(b) and 4(c), respectively. The difference is accounted for by the odd-parity cluster magnetic toroidal dipole in the 120°-AFM structure in Fig. 2(a) [84], which leads to a direct coupling of $\boldsymbol{P} \times \boldsymbol{H}$ [85,86]. In the present case, H_y induces P_x, which results in nonzero $\sigma_{x;yy}^{\mathrm{BCD}}$. Meanwhile, $\sigma_{y;xx}^{\mathrm{BCD}}$ is induced by a secondary effect according to the symmetry lowering under H_y. Nevertheless, the magnitude of $\sigma_{y;xx}^{\mathrm{BCD}}$ is comparable to that of $\sigma_{x;yy}^{\mathrm{BCD}}$ owing to the large enhancement by the band-crossing effect, as discussed in Fig. 3.

IV. SUMMARY

To summarize, we have investigated nonlinear nonreciprocal transport in AFMs without SOC based on microscopic model calculations. We clarified that the noncoplanar spin configuration (local spin scalar chirality) causing the asymmetric band modulation induces Drude-type nonlinear transport, while the collinear spin configuration in the triangle unit induces BCD-type nonlinear transport under an in-plane magnetic field. We showed that the $120°$-AFM spin configurations in the TL and BKL systems are promising candidates to exhibit nonlinear nonreciprocal transport in the external magnetic field. We also presented the essential model parameters in inducing each nonlinear conductivity.

The candidate materials in the present mechanism are $X\mathrm{MnO_3}$ (X = Y, Sc, and Ho) [87–89], $\mathrm{BaCoSiO_4}$ [90], and $\mathrm{Ba_3MnX_2'O_9}$ (X' = Sb and Nb) [91,92], where the noncollinear or noncoplanar AFM structures without spatial inversion symmetry were observed. In addition to the conventional $120°$ AFM structures, it is expected that the Drude-type nonlinear transport appears in other noncoplanar magnets with the local spin scalar chirality degree of freedom, such as the multiple-Q states [15,93,94]. The present results open another route to realize nonlinear transport in magnetic materials, which will stimulate further exploration of functional AFM materials irrespective of the SOC.

[1] T. Kimura, T. Goto, H. Shintani, K. Ishizaka, T. Arima, and Y. Tokura, Nature (London) **426**, 55 (2003).

[2] M. Fiebig, J. Phys. D: Appl. Phys. **38**, R123 (2005).

[3] H. Katsura, N. Nagaosa, and A. V. Balatsky, Phys. Rev. Lett. **95**, 057205 (2005).

[4] M. Mostovoy, Phys. Rev. Lett. **96**, 067601 (2006).

[5] D. Khomskii, Physics **2**, 20 (2009).

[6] Y. Tokura, S. Seki, and N. Nagaosa, Rep. Prog. Phys. **77**, 076501 (2014).

[7] S. Hayami, H. Kusunose, and Y. Motome, Phys. Rev. B **90**, 024432 (2014).

[8] H. Saito, K. Uenishi, N. Miura, C. Tabata, H. Hidaka, T. Yanagisawa, and H. Amitsuka, J. Phys. Soc. Jpn. **87**, 033702 (2018).

[9] F. Thöle and N. A. Spaldin, Philos. Trans. R. Soc. A **376**, 20170450 (2018).

[10] Y. Gao, D. Vanderbilt, and D. Xiao, Phys. Rev. B **97**, 134423 (2018).

[11] A. Shitade, H. Watanabe, and Y. Yanase, Phys. Rev. B **98**, 020407(R) (2018).

[12] S. Mühlbauer, B. Binz, F. Jonietz, C. Pfleiderer, A. Rosch, A. Neubauer, R. Georgii, and P. Böni, Science **323**, 915 (2009).

[13] X. Z. Yu, Y. Onose, N. Kanazawa, J. H. Park, J. H. Han, Y. Matsui, N. Nagaosa, and Y. Tokura, Nature (London) **465**, 901 (2010).

[14] N. Nagaosa and Y. Tokura, Nat. Nanotechnol. **8**, 899 (2013).

[15] S. Hayami and Y. Motome, J. Phys.: Condens. Matter **33**, 443001 (2021).

[16] Y. Tokura, K. Yasuda, and A. Tsukazaki, Nat. Rev. Phys. **1**, 126 (2019).

[17] M. M. Otrokov, I. I. Klimovskikh, H. Bentmann, D. Estyunin, A. Zeugner, Z. S. Aliev, S. Gaß, A. Wolter, A. Koroleva, A. M. Shikin, M. Blanco-Rey, M. Hoffmann, I. P. Rusinov, A. Yu. Vyazovskaya, S. V. Eremeev, Yu. M. Koroteev, V. M. Kuznetsov, F. Freyse, J. Sánchez-Barriga, I. R. Amiraslanov *et al.*, Nature (London) **576**, 416 (2019).

[18] Y. Deng, Y. Yu, M. Z. Shi, Z. Guo, Z. Xu, J. Wang, X. H. Chen, and Y. Zhang, Science **367**, 895 (2020).

[19] V. Bonbien, F. Zhuo, A. Salimath, O. Ly, A. Abbout, and A. Manchon, J. Phys. D: Appl. Phys. **55**, 103002 (2022).

[20] I. Žutić, J. Fabian, and S. Das Sarma, Rev. Mod. Phys. **76**, 323 (2004).

[21] T. Jungwirth, X. Marti, P. Wadley, and J. Wunderlich, Nat. Nanotechnol. **11**, 231 (2016).

[22] V. Baltz, A. Manchon, M. Tsoi, T. Moriyama, T. Ono, and Y. Tserkovnyak, Rev. Mod. Phys. **90**, 015005 (2018).

[23] N. Nagaosa, J. Sinova, S. Onoda, A. H. MacDonald, and N. P. Ong, Rev. Mod. Phys. **82**, 1539 (2010).

[24] L. Šmejkal, A. H. MacDonald, J. Sinova, S. Nakatsuji, and T. Jungwirth, Nat. Rev. Mater. **7**, 482 (2022).

[25] R. Karplus and J. M. Luttinger, Phys. Rev. **95**, 1154 (1954).

[26] J. Smit, Physica **24**, 39 (1958).

[27] F. E. Maranzana, Phys. Rev. **160**, 421 (1967).

[28] L. Berger, Phys. Rev. B **2**, 4559 (1970).

[29] P. Nozieres and C. Lewiner, J. Phys. France **34**, 901 (1973).

[30] T. Jungwirth, Q. Niu, and A. H. MacDonald, Phys. Rev. Lett. **88**, 207208 (2002).

[31] I. V. Solovyev, Phys. Rev. B **55**, 8060 (1997).

[32] L. Šmejkal, R. González-Hernández, T. Jungwirth, and J. Sinova, Sci. Adv. **6**, eaaz8809 (2020).

[33] D.-F. Shao, J. Ding, G. Gurung, S.-H. Zhang, and E. Y. Tsymbal, Phys. Rev. Applied **15**, 024057 (2021).

[34] K. Samanta, M. Ležaić, M. Merte, F. Freimuth, S. Blügel, and Y. Mokrousov, J. Appl. Phys. **127**, 213904 (2020).

[35] M. Naka, S. Hayami, H. Kusunose, Y. Yanagi, Y. Motome, and H. Seo, Phys. Rev. B **102**, 075112 (2020).

[36] S. Hayami and H. Kusunose, Phys. Rev. B **103**, L180407 (2021).

[37] T. Tomizawa and H. Kontani, Phys. Rev. B **80**, 100401(R) (2009).

[38] H. Chen, Q. Niu, and A. H. MacDonald, Phys. Rev. Lett. **112**, 017205 (2014).

[39] S. Nakatsuji, N. Kiyohara, and T. Higo, Nature (London) **527**, 212 (2015).

[40] M.-T. Suzuki, T. Koretsune, M. Ochi, and R. Arita, Phys. Rev. B **95**, 094406 (2017).

[41] H. Chen, T.-C. Wang, D. Xiao, G.-Y. Guo, Q. Niu, and A. H. MacDonald, Phys. Rev. B **101**, 104418 (2020).

[42] F. R. Lux, F. Freimuth, S. Blügel, and Y. Mokrousov, Phys. Rev. Lett. **124**, 096602 (2020).

[43] K. Ohgushi, S. Murakami, and N. Nagaosa, Phys. Rev. B **62**, R6065 (2000).

[44] R. Shindou and N. Nagaosa, Phys. Rev. Lett. **87**, 116801 (2001).

[45] Y. Taguchi, Y. Oohara, H. Yoshizawa, N. Nagaosa, and Y. Tokura, Science **291**, 2573 (2001).

[46] I. Martin and C. D. Batista, Phys. Rev. Lett. **101**, 156402 (2008).

[47] A. Neubauer, C. Pfleiderer, B. Binz, A. Rosch, R. Ritz, P. G. Niklowitz, and P. Böni, Phys. Rev. Lett. **102**, 186602 (2009).

[48] D. Loss and P. M. Goldbart, Phys. Rev. B **45**, 13544 (1992).

[49] J. Ye, Y. B. Kim, A. J. Millis, B. I. Shraiman, P. Majumdar, and Z. Tešanović, Phys. Rev. Lett. **83**, 3737 (1999).

[50] F. D. M. Haldane, Phys. Rev. Lett. **93**, 206602 (2004).

[51] D. Xiao, M.-C. Chang, and Q. Niu, Rev. Mod. Phys. **82**, 1959 (2010).

[52] S.-S. Zhang, H. Ishizuka, H. Zhang, G. B. Halász, and C. D. Batista, Phys. Rev. B **101**, 024420 (2020).

[53] G. Tatara and H. Kawamura, J. Phys. Soc. Jpn. **71**, 2613 (2002).

[54] C. D. Batista, S.-Z. Lin, S. Hayami, and Y. Kamiya, Rep. Prog. Phys. **79**, 084504 (2016).

[55] Y. Gao, S. A. Yang, and Q. Niu, Phys. Rev. Lett. **112**, 166601 (2014).

[56] I. Sodemann and L. Fu, Phys. Rev. Lett. **115**, 216806 (2015).

[57] D. E. Parker, T. Morimoto, J. Orenstein, and J. E. Moore, Phys. Rev. B **99**, 045121 (2019).

[58] C. Xiao, Z. Z. Du, and Q. Niu, Phys. Rev. B **100**, 165422 (2019).

[59] S. Nandy and I. Sodemann, Phys. Rev. B **100**, 195117 (2019).

[60] Y. Tokura and N. Nagaosa, Nat. Commun. **9**, 3740 (2018).

[61] Y. Gao, Front. Phys. **14**, 33404 (2019).

[62] M. Yatsushiro, H. Kusunose, and S. Hayami, Phys. Rev. B **104**, 054412 (2021).

[63] R. Oiwa and H. Kusunose, J. Phys. Soc. Jpn. **91**, 014701 (2022).

[64] Y. Togawa, Y. Kousaka, K. Inoue, and J.-i. Kishine, J. Phys. Soc. Jpn. **85**, 112001 (2016).

[65] H. Ishizuka and N. Nagaosa, Nat. Commun. **11**, 2986 (2020).

[66] T. Holder, D. Kaplan, and B. Yan, Phys. Rev. Research **2**, 033100 (2020).

[67] R. Fei, W. Song, and L. Yang, Phys. Rev. B **102**, 035440 (2020).

[68] H. Watanabe and Y. Yanase, Phys. Rev. Research **2**, 043081 (2020).

[69] H. Watanabe and Y. Yanase, Phys. Rev. X **11**, 011001 (2021).

[70] M. Yatsushiro, R. Oiwa, H. Kusunose, and S. Hayami, Phys. Rev. B **105**, 155157 (2022).

[71] C. Wang, Y. Gao, and D. Xiao, Phys. Rev. Lett. **127**, 277201 (2021).

[72] H. Liu, J. Zhao, Y.-X. Huang, W. Wu, X.-L. Sheng, C. Xiao, and S. A. Yang, Phys. Rev. Lett. **127**, 277202 (2021).

[73] P. Sahebsara and D. Sénéchal, Phys. Rev. Lett. **100**, 136402 (2008).

[74] T. Yoshioka, A. Koga, and N. Kawakami, Phys. Rev. Lett. **103**, 036401 (2009).

[75] H.-Y. Yang, A. M. Läuchli, F. Mila, and K. P. Schmidt, Phys. Rev. Lett. **105**, 267204 (2010).

[76] Y. Akagi and Y. Motome, J. Phys. Soc. Jpn. **79**, 083711 (2010).

[77] S. Hayami, M. Udagawa, and Y. Motome, J. Phys. Soc. Jpn. **80**, 073704 (2011).

[78] S. Hayami, Y. Yanagi, and H. Kusunose, Phys. Rev. B **101**, 220403(R) (2020).

[79] S. Hayami, Y. Yanagi, and H. Kusunose, Phys. Rev. B **102**, 144441 (2020).

[80] L.-D. Yuan, Z. Wang, J.-W. Luo, and A. Zunger, Phys. Rev. Materials **5**, 014409 (2021).

[81] J. Kim, K.-W. Kim, D. Shin, S.-H. Lee, J. Sinova, N. Park, and H. Jin, Nat. Commun. **10**, 3965 (2019).

[82] L. N. Bulaevskii, C. D. Batista, M. V. Mostovoy, and D. I. Khomskii, Phys. Rev. B **78**, 024402 (2008).

[83] In the case of the collinear spin configuration, $\sigma_{y;xx}^{\text{BCD}}$ becomes nonzero without H_y.

[84] M.-T. Suzuki, T. Nomoto, R. Arita, Y. Yanagi, S. Hayami, and H. Kusunose, Phys. Rev. B **99**, 174407 (2019).

[85] N. A. Spaldin, M. Fiebig, and M. Mostovoy, J. Phys.: Condens. Matter **20**, 434203 (2008).

[86] S. Hayami, M. Yatsushiro, Y. Yanagi, and H. Kusunose, Phys. Rev. B **98**, 165110 (2018).

[87] A. Muñoz, J. A. Alonso, M. J. Martínez-Lope, M. T. Casáis, J. L. Martínez, and M. T. Fernández-Díaz, Phys. Rev. B **62**, 9498 (2000).

[88] A. Munoz, J. Alonso, M. Martínez-Lope, M. Casáis, J. Martínez, and M. Fernandez-Diaz, Chem. Mater. **13**, 1497 (2001).

[89] P. Brown and T. Chatterji, J. Phys.: Condens. Matter **18**, 10085 (2006).

[90] L. Ding, X. Xu, H. O. Jeschke, X. Bai, E. Feng, A. S. Alemayehu, J. Kim, F.-T. Huang, Q. Zhang, X. Ding, N. Harrison, V. Zapf, D. Khomskii, I. I. Mazin, S.-W. Cheong, and H. Cao, Nat. Commun. **12**, 5339 (2021).

[91] Y. Doi, Y. Hinatsu, and K. Ohoyama, J. Phys.: Condens. Matter **16**, 8923 (2004).

[92] M. Lee, E. S. Choi, X. Huang, J. Ma, C. R. Dela Cruz, M. Matsuda, W. Tian, Z. L. Dun, S. Dong, and H. D. Zhou, Phys. Rev. B **90**, 224402 (2014).

[93] S. Hayami, T. Okubo, and Y. Motome, Nat. Commun. **12**, 6927 (2021).

[94] S. Hayami and R. Yambe, Phys. Rev. Research **3**, 043158 (2021).